


Cite this: *RSC Adv.*, 2020, 10, 8444

# Rationalization of the X-ray photoelectron spectroscopy of aluminium phosphates synthesized from different precursors†

Victoria Bemmer,<sup>id d</sup> Michael Bowker,<sup>id a</sup> James H. Carter,<sup>id a</sup> Philip R. Davies,<sup>id \*a</sup> Lee E. Edwards,<sup>id a</sup> Kenneth D. M. Harris,<sup>id b</sup> Colan E. Hughes,<sup>b</sup> Fiona Robinson,<sup>id c</sup> David J. Morgan<sup>id a</sup> and Matthew G. Thomas<sup>a</sup>

The aim of this paper is to clarify the assignments of X-ray photoelectron spectra of aluminium phosphate materials prepared from the reaction of phosphoric acid with three different aluminium precursors [Al(OH)<sub>3</sub>, Al(NO<sub>3</sub>)<sub>3</sub> and AlCl<sub>3</sub>] at different annealing temperatures. The materials prepared have been studied by X-ray photoelectron spectroscopy (XPS), powder X-ray diffraction (XRD), infrared spectroscopy and high-resolution solid-state <sup>31</sup>P NMR spectroscopy. A progressive polymerization from orthophosphate to metaphosphates is observed by XRD, ATR-FTIR and solid state <sup>31</sup>P NMR, and on this basis the oxygen states observed in the XP spectra at 532.3 eV and 533.7 eV are assigned to P–O–Al and P–O–P environments, respectively. The presence of cyclic polyphosphates at the surface of the samples is also evident.

Received 24th October 2019  
Accepted 10th February 2020

DOI: 10.1039/c9ra08738a

rsc.li/rsc-advances

## Introduction

There are a wide array of applications of phosphate based materials, including biomedical (due to the natural occurrence of phosphates in physiology and their biocompatibility<sup>1–4</sup>), ceramics (due to their high strength and thermal stability) and refractory materials (in which phosphates are frequently used as binders<sup>5</sup>). Curing temperatures of phosphates are critical to their performance in the latter applications and as a result there has been a concerted effort to understand the thermal evolution of phosphate systems. Heating induces a progressive polymerization starting from orthophosphates (PO<sub>4</sub><sup>3–</sup>), which polymerize to form a series of polyphosphates such as the pyrophosphates (P<sub>2</sub>O<sub>7</sub><sup>4–</sup>) and finally metaphosphates, which are long range cross-linked networks (PO<sub>3</sub><sup>–</sup>)<sub>n</sub>.<sup>6</sup> This paper is focused on aluminium phosphates generated from a mixture of phosphoric acid and three different aluminium based precursors: Al(OH)<sub>3</sub>, Al(NO<sub>3</sub>)<sub>3</sub> and AlCl<sub>3</sub>.

The majority of studies on aluminium phosphates have focused on bulk analysis techniques,<sup>7</sup> such as powder X-ray

diffraction (XRD), solid-state <sup>31</sup>P NMR, FTIR and thermogravimetric methods, but the surface properties of these materials are also of interest and one of the most commonly used techniques to investigate this aspect is X-ray photoelectron spectroscopy (XPS). A seminal study by Gresch *et al.*<sup>8</sup> in 1979 on XPS of sodium phosphates provided well substantiated peak assignments for the oxygen region. This paper has since been extensively cited and used as a benchmark for XPS studies of phosphates. Gresch *et al.* proposed that the different states of oxygen created by crosslinking between phosphate units could be distinguished by their XP spectra, with the “bridging” oxygens appearing at higher binding energy (533.1–533.6 eV) than “non-bridging” oxygens (530.5–531.7 eV). This assignment was based on electronegativity arguments and spectra of model compounds. Concomitant with the shift in O(1s) binding energy, Gresch *et al.* reported that the P(2p) binding energy shifts from 132.5 eV to 134.5 eV as the degree of P–O–P bridging bonds increases.

More recently, Crobu *et al.*<sup>9</sup> have also used the shift in O(1s) binding energy to assess the ratio of bridging to non-bridging oxygen in zinc polyphosphate glasses, correlating their results with secondary ion mass spectrometry measurements. They reported a shift from 532.2 eV to 534.0 eV as the reference material changed from an orthophosphate to a metaphosphate, with the P(2p) peak shifting from 134.0 eV to 134.8 eV.

Rotole and Sherwood, on the other hand, studied electrochemically deposited phosphate films on aluminium substrates.<sup>10</sup> The XP spectra were referenced against data on aluminium orthophosphate<sup>11</sup> and metaphosphate<sup>12</sup> samples. They reported a constant P(2p) binding energy of 134.5 eV and

<sup>a</sup>Cardiff Catalysis Institute, School of Chemistry, Cardiff University, Cardiff, CF10 3AT, UK. E-mail: daviespr@cardiff.ac.uk

<sup>b</sup>School of Chemistry, Cardiff University, Cardiff, CF10 3AT, UK

<sup>c</sup>Cogent Power Ltd, Newport NP19 0RB, UK

<sup>d</sup>Dept. of Materials, Imperial College, South Kensington Campus, London SW7 2AZ, UK

† Electronic supplementary information (ESI) available. See DOI: 10.1039/c9ra08738a

‡ Current address: Dept. of Materials, Imperial College, South Kensington Campus, London SW7 2AZ, UK.



a shift in the O(1s) peak from 531.4 eV for the orthophosphate to a broader peak at 531.8 eV for the metaphosphate. The latter peak clearly showed evidence for a second component at about 533.5 eV. However, the O(1s) data from the electrochemically treated surface were not so conclusive; the O(1s) spectrum of the “metaphosphate” was significantly broader than that of the orthophosphate and seemed to consist of two components. It is not clear whether the component due to bridging oxygens is at higher or lower binding energy than the component due to terminal oxygens.

In the present study, we have used solid-state  $^{31}\text{P}$  NMR, powder XRD and FTIR data to explore the structural changes that occur in aluminium phosphate materials synthesized from 3 : 1 mixtures of phosphoric acid and an aluminium precursor (either aluminium hydroxide, aluminium nitrate or aluminium chloride), which throw light on the information available from the surface specific XPS technique. Our results show that the expected polymerization occurs in materials prepared from all three precursors, and largely confirm the assignments of XP spectra based on existing literature. However, we also find evidence for the presence, at the surface, of polyphosphate species that do not contain aluminium, which distorts the Al : O : P ratios established from the XPS spectra.

## Experimental

### Synthesis of aluminium phosphate powders

The aluminium precursor  $\text{AlX}_3$ , where X = OH (Sigma-Aldrich, Reagent Grade),  $\text{NO}_3$  (Sigma-Aldrich, ACS Reagent, >98%) or Cl (Sigma-Aldrich, 99.99%), was added to water (50 ml) at 298 K and mixed until dissolved.  $\text{H}_3\text{PO}_4$  (8.75 ml, Sigma-Aldrich, 85% wt, 99.99% purity) was added to the  $\text{AlX}_3$  solution to give a P : Al ratio of 3 : 1 and the solution was allowed to mix for 30 min. The reaction mixture was then heated on a hotplate to evaporate the water, resulting in the formation of a viscous gel. Separate samples of the gel were heated in air in a furnace for a period of one hour at three different temperatures (300, 500 and 800 °C), and then allowed to cool to room temperature before analysis. In the case of the materials prepared from  $\text{Al}(\text{OH})_3$  and  $\text{Al}(\text{NO}_3)_3$ , a slightly wet white powder was obtained on heating to 300 °C which was observed (by eye) to dry completely on heating at the higher temperatures. However, the samples prepared from  $\text{AlCl}_3$  remained gel-like at 300 °C. These samples were stable under vacuum and so could be analysed by XPS, but they had to be heated to 400 °C to obtain a solid that was suitable for analysis by solid-state NMR and ATR could be obtained. In the discussion below, the materials prepared from the  $\text{Al}(\text{OH})_3$ ,  $\text{Al}(\text{Cl})_3$  and  $\text{Al}(\text{NO}_3)_3$  precursors are labelled  $\text{AlP}_{\text{OH}}$ ,  $\text{AlP}_{\text{Cl}}$  and  $\text{AlP}_{\text{NO}_3}$ , respectively.

### Materials characterization

XP spectra were recorded at room temperature on the powder samples using a Kratos Axis Ultra-DLD photoelectron spectrometer with a monochromatic Al K $\alpha$  X-ray source in the “hybrid spectroscopy” mode resulting in an analysis area of 700  $\times$  300  $\mu\text{m}^2$  at a pass-energy of 40 eV for high-resolution scans

and 160 eV for survey scans. The XPS data were analysed using CasaXPS<sup>13</sup> with all binding energies referenced to the C(1s) peak at 284.7 eV with an uncertainty of  $\sim 0.2$  eV. Since intensities for powder samples are dependent on the surface area analysed, which is poorly reproducible between different powder samples, the XP spectra shown in the figures are normalized to the point of maximum intensity. Curve fits were made using Gaussian–Lorentzian (GL (30)) line-shapes.

Powder X-ray diffraction (XRD) data were recorded at room temperature using a PANalytical X'Pert Pro diffractometer with a monochromatic Cu K $\alpha$  source ( $\lambda = 0.154$  nm) operating at 40 kV and 40 mA. The data were recorded over the  $2\theta$  range 10–80° with a step size of 0.016°.

High-resolution solid-state  $^{31}\text{P}$  NMR spectra were acquired at room temperature on a Chemagnetics Infinity Plus spectrometer ( $^{31}\text{P}$  Larmor frequency, 121.50 MHz). The samples were contained in a 4 mm rotor with magic-angle spinning at 12 kHz. Methyltriphenylphosphine oxide (MDPPO) was used as a reference, with  $^{31}\text{P}$  chemical shift at 30.8 ppm.

FTIR spectra were recorded using a germanium crystal ATR on a Varian 3100 Excalibur system with Varian Resolutions Pro software.

## Results

### Bulk structural analysis using FTIR, XRD and solid-state $^{31}\text{P}$ NMR

Throughout the discussion, we refer to each sample by the notation  $\text{AlP}_{\text{OH}}(T)$ ,  $\text{AlP}_{\text{Cl}}(T)$  or  $\text{AlP}_{\text{NO}_3}(T)$ , where the subscript identifies the precursor used in the synthesis and  $T$  denotes the annealing temperature. All the analysis was performed after cooling to room temperature.

The crystalline phases present within each sample were investigated by powder XRD. Fig. 1, shows the XRD patterns for the  $\text{AlP}_{\text{OH}}$  samples. For  $\text{AlP}_{\text{OH}}(300)$  [*i.e.*, the sample prepared from the  $\text{Al}(\text{OH})_3$  precursor and annealed at 300 °C], only low intensity peaks are observed in the XRD data, and we have been unable to definitively match these peaks to a known structure. For the  $\text{AlP}_{\text{OH}}(500)$  sample, the XRD data show sufficient crystallinity to allow Le Bail fitting, although Rietveld refinement was not possible. The Le Bail fitting confirms that two distinct phases are present: a cubic aluminium metaphosphate [ $\text{Al}(\text{PO}_3)_3$ ] (ICSD: 26759) and an aluminium hexacyclophosphate (ICSD: 260723). For the  $\text{AlP}_{\text{OH}}(800)$  sample, only the cubic aluminium metaphosphate is present. The results from Le Bail fitting are shown in Fig. S1 and S2 (in ESI†).

d'Yvoire<sup>14,15</sup> also reported a pure cubic phase for a material prepared from  $\text{Al}(\text{OH})_3$  and annealed at 800 °C, with a second phase present in the material annealed at 500 °C. However, d'Yvoire assigned the second phase to a monoclinic structure rather than the aluminium hexacyclophosphate observed here.

XRD indicates that the  $\text{AlP}_{\text{NO}_3}(500)$  and  $\text{AlP}_{\text{NO}_3}(800)$  samples (Fig. S3 and S4†) are a mixture of the cubic aluminium metaphosphate and aluminium hexacyclophosphate phases [similar to  $\text{AlP}_{\text{OH}}(500)$  but different from  $\text{AlP}_{\text{OH}}(800)$ ]. Among the samples prepared from the  $\text{AlCl}_3$  precursor, the only crystalline

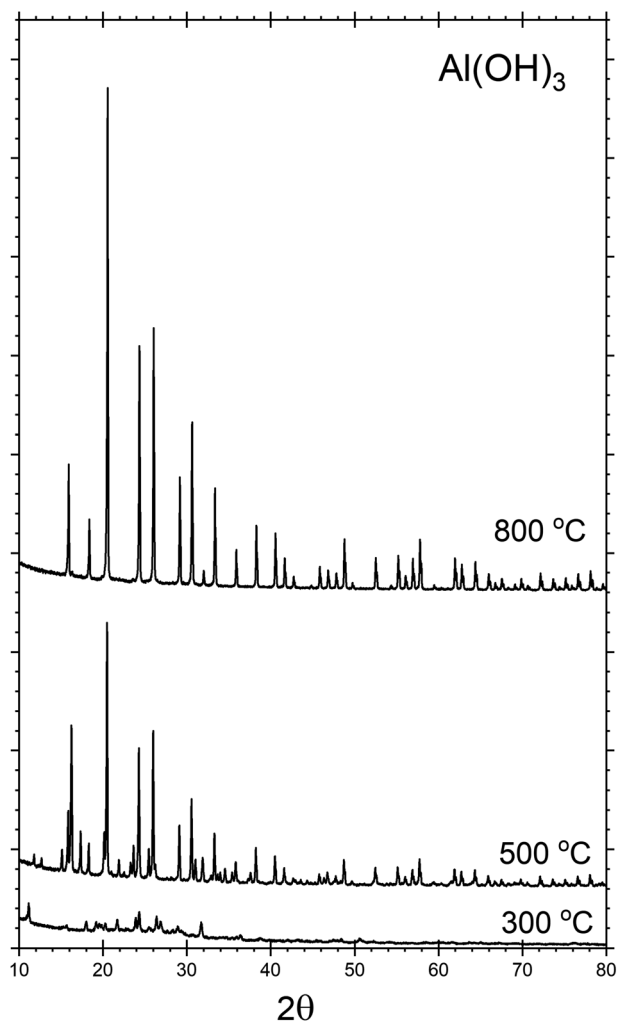


Fig. 1 Powder XRD patterns recorded for the  $\text{AlPO}_\text{OH}$  materials, with annealing at different temperatures. The  $\text{AlPO}_\text{OH}(300)$  sample is mostly non-crystalline, but both cubic metaphosphate and hexacyclopophosphate are present in the  $\text{AlPO}_\text{OH}(500)$  sample. The  $\text{AlPO}_\text{OH}(800)$  sample is a pure phase of the cubic metaphosphate. Data for the  $\text{AlPO}_\text{Cl}$  and  $\text{AlPO}_\text{NO}_3$  materials are given in ESI.†

product was  $\text{AlPO}_\text{Cl}(800)$ , identified from XRD as pure cubic  $\text{Al}(\text{PO}_3)_3$  (Fig. S5†).

Further structural insights are obtained from high-resolution solid-state  $^{31}\text{P}$  NMR spectra (Fig. 2). For several of the samples, a peak at 0 ppm is present and assigned as the phosphoric acid starting material. As the annealing temperature increases, there is a trend towards increasingly negative  $^{31}\text{P}$  chemical shifts, attributed to polymerization.<sup>16</sup> For  $\text{AlPO}_\text{OH}(300)$ , a broad set of overlapping peaks is observed between 5 ppm and  $-40$  ppm, possibly suggesting an amorphous structure. The peaks at  $-21$  ppm and  $-32$  ppm (which represent *ca.* 20% of the total signal) are assigned<sup>16</sup> to aluminium tripolyphosphate ( $\text{AlH}_2\text{P}_3\text{O}_{10} \cdot \text{H}_2\text{O}$ ). These peaks are also observed for  $\text{AlPO}_\text{NO}_3(300)$ . For  $\text{AlPO}_\text{OH}(800)$ , only one peak is observed (at 50.5 ppm) and is attributed unambiguously to cubic  $\text{Al}(\text{PO}_3)_3$ , consistent with the presence of a single phosphorus environment in this structure (Fig. 3). This peak is also present for the

$\text{AlPO}_\text{OH}(500)$  sample, together with peaks at  $-36.5$  ppm and  $-43.0$  ppm; the area ratio for these two peaks is 2 : 1, consistent with the presence of three crystallographically distinct phosphorus environments in the aluminium hexacyclopophosphate phase (Fig. 3). Monoclinic  $\text{Al}(\text{PO}_3)_3$ , on the other hand, has 9 distinct phosphorus environments (Fig. 3).

For the  $\text{AlPO}_\text{NO}_3(300)$  sample, three peaks are observed between 5 ppm and  $-35$  ppm [in contrast to the overlapping set of peaks observed in this region for  $\text{AlPO}_\text{OH}(300)$ ], including peaks at  $-21$  ppm and  $-32$  ppm assigned to aluminium tripolyphosphate ( $\text{AlH}_2\text{P}_3\text{O}_{10} \cdot \text{H}_2\text{O}$ ), which represents  $\sim 50\%$  of the signal. The peak at  $-3.4$  ppm is attributed to some remaining aluminium orthophosphate. For the  $\text{AlPO}_\text{NO}_3(500)$  sample, the  $^{31}\text{P}$  NMR spectrum contains peaks characteristic of the hexacyclopophosphate (43.3%) and cubic metaphosphate (52%). Annealing at a higher temperature does not complete the transformation to the cubic metaphosphate as the  $^{31}\text{P}$  NMR spectrum for the  $\text{AlPO}_\text{NO}_3(800)$  sample clearly contains peaks due to the hexacyclopophosphate phase (*ca.* 36% of the signal intensity).

The  $^{31}\text{P}$  NMR spectra for  $\text{AlPO}_\text{Cl}(400)$  and  $\text{AlPO}_\text{Cl}(500)$  are significantly different from those observed for the  $\text{AlPO}_\text{OH}$  and  $\text{AlPO}_\text{NO}_3$  materials. The major peaks are due to cubic metaphosphate (50.5 ppm), orthophosphate (1 ppm and 0 ppm), pyrophosphate ( $-12$  ppm and  $-13.5$  ppm) and polyphosphate (peaks in the range  $-20$  ppm to  $-28$  ppm), with only very weak peaks observed for hexacyclopophosphate. In contrast, the  $\text{AlPO}_\text{Cl}(800)$  sample is a pure phase of cubic  $\text{Al}(\text{PO}_3)_3$ . These observations suggest that the metaphosphate formed from the  $\text{AlCl}_3$  precursor may be produced *via* a slightly different pathway than from the  $\text{Al}(\text{OH})_3$  and  $\text{Al}(\text{NO}_3)_3$  precursors. We deduce that the stability of the Al–Cl bond hinders formation of aluminium phosphate from the  $\text{Al}(\text{Cl})_3$  precursor at lower temperatures, leaving the phosphoric acid to react mostly with itself to form varying degrees of polyphosphates. However, at the higher annealing temperature of  $800^\circ\text{C}$ , the phosphate transforms completely to cubic  $\text{Al}(\text{PO}_3)_3$ .

### Surface analysis with XPS

The XP spectra in Fig. 4 show the O(1s) data for all samples. For samples prepared from each of the three precursors, there is a general shift in peak position towards *lower* binding energy as the annealing temperature is increased. Curve fitting confirms that two distinguishable peaks are present at binding energies of *ca.* 533.7 eV and 532.3 eV in all spectra, with a transfer of intensity from the higher binding energy peak to the lower binding energy peak as the annealing temperature is increased (peak area ratios are given in Table 1). In particular, we note the close similarity between the spectra for the  $\text{AlPO}_\text{OH}(800)$ ,  $\text{AlPO}_\text{NO}_3(800)$  and  $\text{AlPO}_\text{Cl}(800)$  samples, all of which show an approximately 2 : 1 intensity ratio (lower : higher binding energy peaks) and resemble the O(1s) spectrum of aluminium metaphosphate published by Rotole and Sherwood.<sup>12</sup>

The Al(2p) XP spectra for all samples are shown in Fig. 5. For the  $\text{AlPO}_\text{OH}$  samples, a strong peak is present for all annealing temperatures at  $\sim 75.3$  eV for  $\text{AlPO}_\text{OH}(300)$  and shifting slightly to



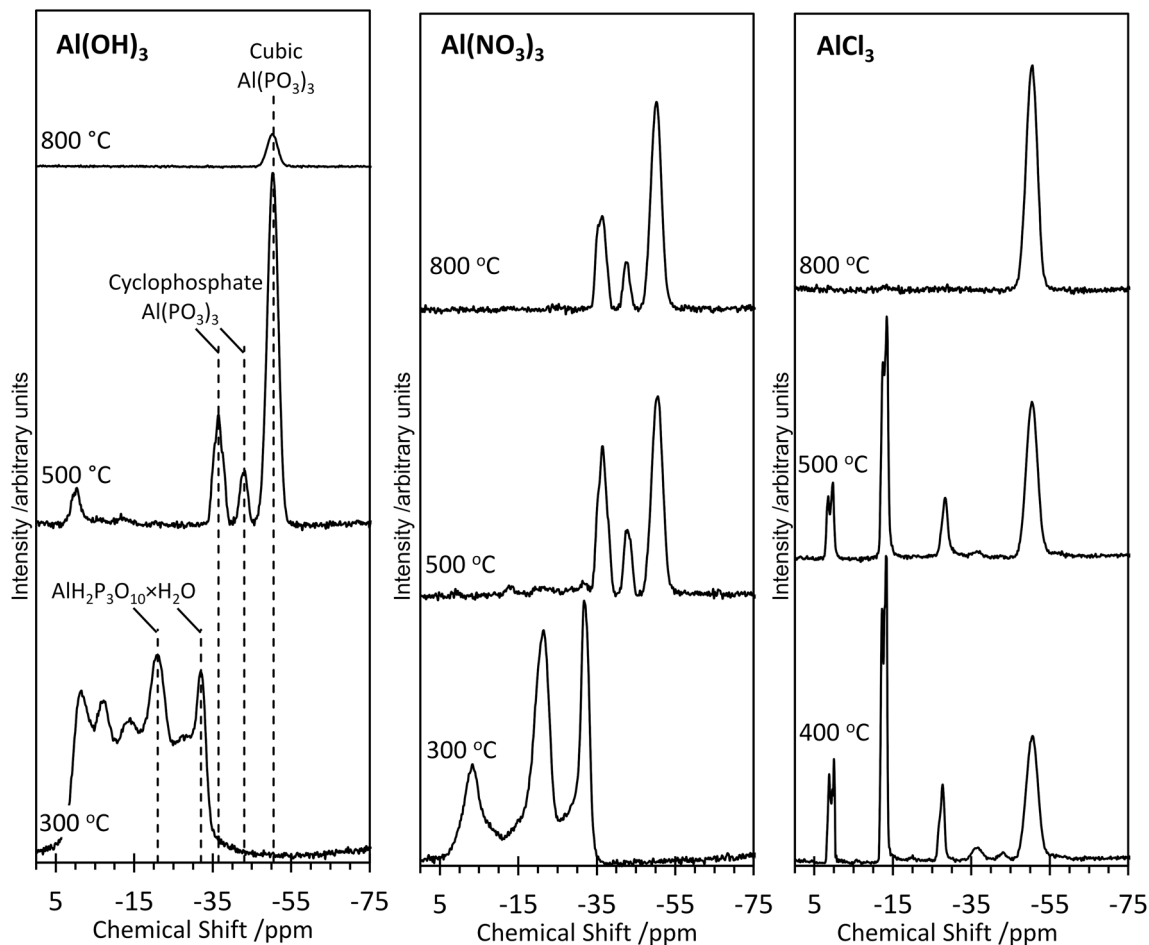


Fig. 2 High-resolution solid-state  $^{31}\text{P}$  NMR spectra of the aluminium phosphate materials prepared from the  $\text{Al}(\text{OH})_3$ ,  $\text{Al}(\text{NO}_3)_3$  and  $\text{AlCl}_3$  precursors at different annealing temperatures. All spectra were recorded at room temperature.

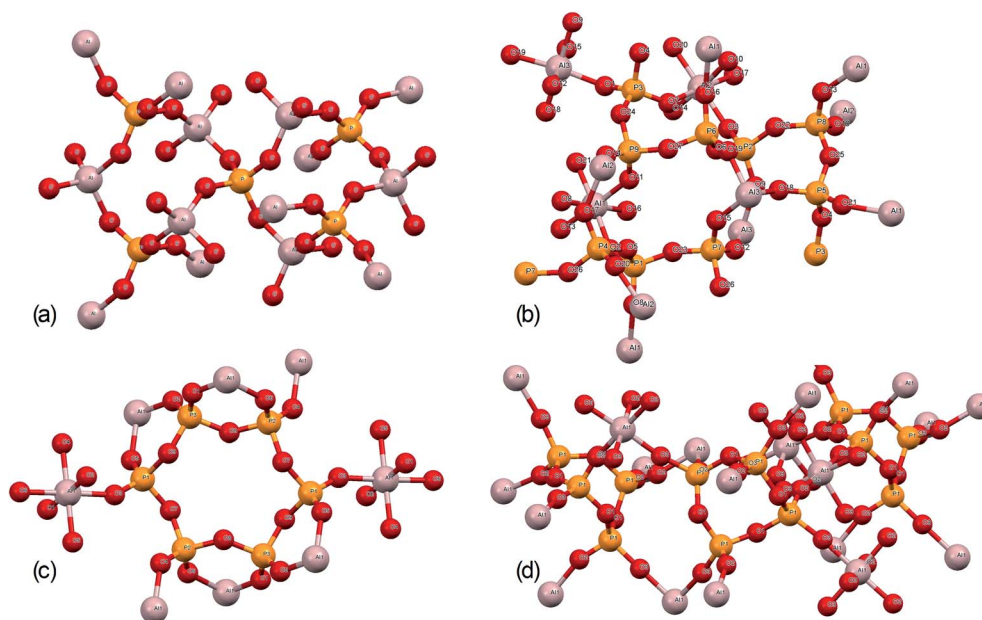


Fig. 3 Structures of (a) aluminium orthophosphate ( $\text{AlPO}_4$ ), (b) monoclinic aluminium metaphosphate, (c) aluminium hexacyclophosphate, and (d) cubic aluminium metaphosphate.



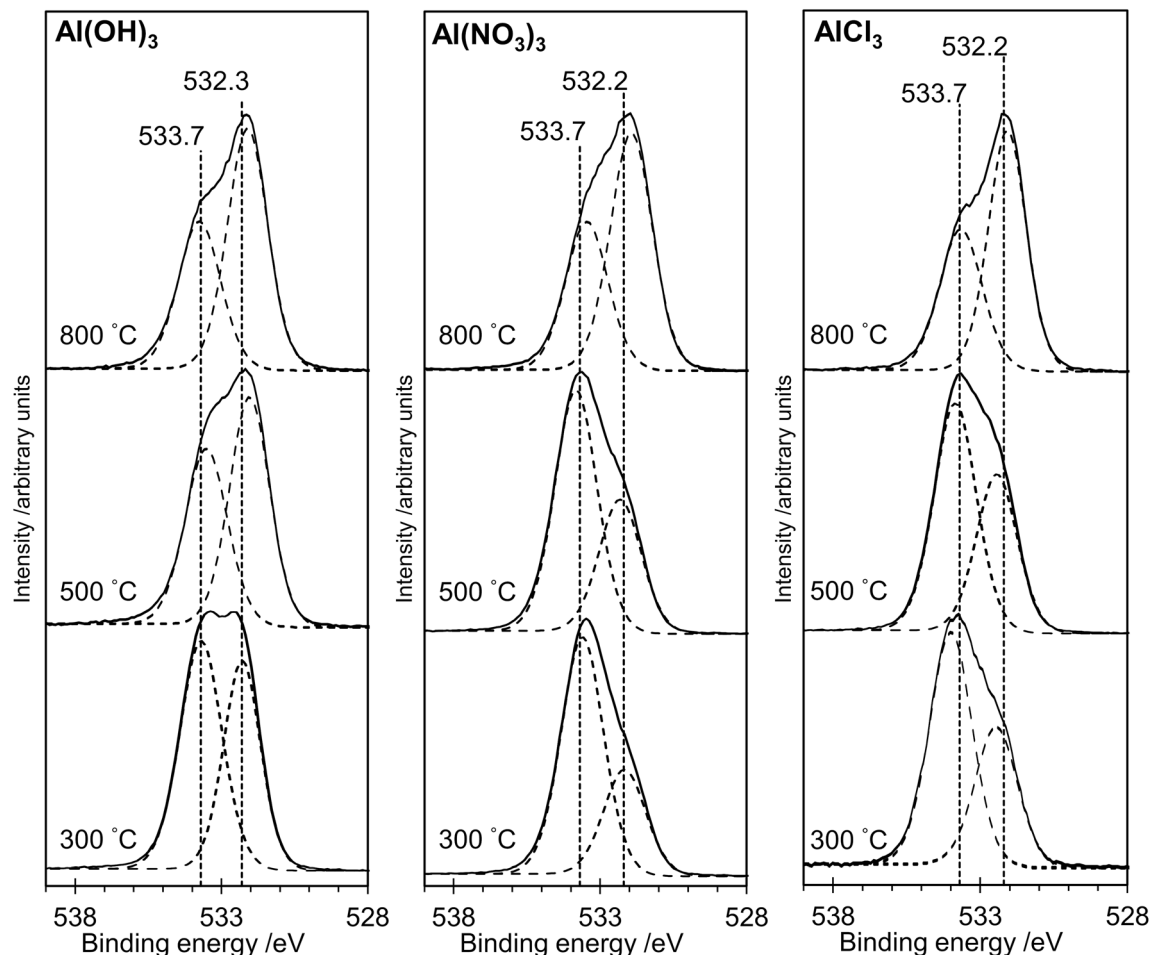


Fig. 4 X-ray photoelectron spectra in the O(1s) region for the aluminium phosphate materials prepared from the  $\text{Al}(\text{OH})_3$ ,  $\text{Al}(\text{NO}_3)_3$  and  $\text{AlCl}_3$  precursors at different annealing temperatures. Solid lines show experimental data. The dotted curves show deconvolution using the methods described in the text. For all three precursors, the intensity of the peak at lower binding energy increases relative to the peak at higher binding energy as the annealing temperature is increased.

Table 1 Quantification of XP spectra

Reactant		Annealing temperature/°C					
		300/400		500		800	
$\text{Al}(\text{OH})_3$	O(1s) binding energy <sup>a</sup>	533.7	532.3	533.5	532.0	533.8	532.1
	% of peak area	55.5	44.5	44.6	55.4	39.0	61.0
	~532 : 533 ratio	0.8		1.2		1.6	
	O : P ratio	3.2		2.9		3.0	
	P : Al ratio	5.3		5		3.8	
$\text{Al}(\text{NO}_3)_3$	O(1s) binding energy <sup>a</sup>	533.6	532.2	533.8	532.3	533.7	532.1
	% of peak area	69.1	30.9	64.4	35.6	38.5	61.5
	~532 : 533 ratio	0.43		0.55		1.6	
	O : P ratio	2.8		3		2.9	
	P : Al ratio	n/a		10.2		3.6	
$\text{AlCl}_3$	O(1s) binding energy <sup>a</sup>	534.0	532.5	533.9	532.4	533.7	532.1
	~532 : 533 ratio	62.4	37.6	59.8	40.2	39.6	60.4
	Peak area ratio	0.6		0.7		1.5	
	O : P ratio	3.3		3.1		2.8	
	P : Al ratio	n/a		n/a		4.6	

<sup>a</sup> Binding energies are referenced to the C (1s) peak at 284.7 eV; curves are fitted with Gaussian–Lorentzian (GL (30)) line shapes.



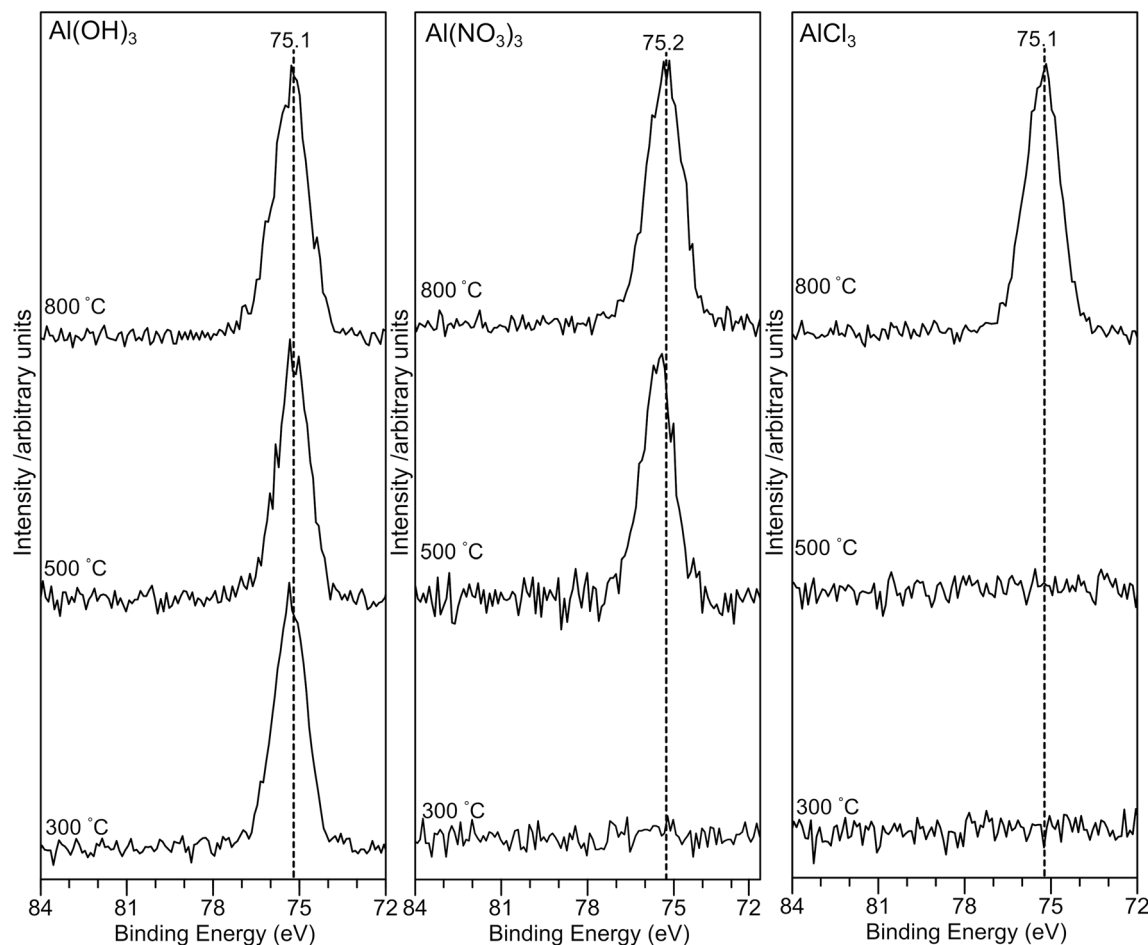


Fig. 5 X-ray photoelectron spectra in the Al(2p) region for the aluminium phosphate materials prepared from the  $\text{Al}(\text{OH})_3$ ,  $\text{Al}(\text{NO}_3)_3$  and  $\text{AlCl}_3$  precursors at different annealing temperatures. The absence of any Al(2p) signal for lower annealing temperatures in the case of the  $\text{Al}(\text{NO}_3)_3$  and  $\text{AlCl}_3$  precursors suggests that the surface is dominated by a hydrogen polyphosphate.

75.1 eV for  $\text{AlP}_{\text{OH}}(800)$ . However, for the  $\text{AlP}_{\text{NO}_3}(300)$  sample, no peaks are observed in the Al(2p) XP spectrum, while a peak at *ca.* 75 eV is present for both  $\text{AlP}_{\text{NO}_3}(500)$  and  $\text{AlP}_{\text{NO}_3}(800)$ . For the  $\text{AlP}_{\text{Cl}}$  samples, again no peaks are observed in the Al(2p) XP spectra for the  $\text{AlP}_{\text{Cl}}(300)$  and  $\text{AlP}_{\text{Cl}}(500)$  samples, while a peak is observed at *ca.* 75 eV for  $\text{AlP}_{\text{Cl}}(800)$ . This difference in behaviour parallels the physical appearance of the  $\text{AlP}_{\text{Cl}}$  samples, for which both  $\text{AlP}_{\text{Cl}}(300)$  and  $\text{AlP}_{\text{Cl}}(500)$  are tacky but  $\text{AlP}_{\text{Cl}}(800)$  is not.

The XP spectra in the P(2p) region (Fig. 6) have a single peak at  $\sim 134.8$  eV for all samples with a small shift ( $\sim 0.2$  eV) to lower binding energy as the annealing temperature is increased to 800 °C. The observed peak is consistent with the average peak position for metaphosphates in the NIST database<sup>17</sup> (134.8 eV;  $\sigma = 0.5$  eV) and with results of Rotole and Sherwood<sup>10,11</sup> on aluminium phosphates. However, it is in marked contrast to sodium phosphates,<sup>8</sup> for which the P(2p) binding energy shifts by 2 eV from the orthophosphate (132.5 eV) to the oxygen-bridged metaphosphate (134.5 eV).

The atomic ratios calculated from the XPS spectra (Table 1) are informative. The P : O ratio is very close to 1 : 3 for all samples but the P : Al ratio is always higher than 3 : 1. The fact

that the XPS survey scans for materials prepared at lower annealing temperatures (Fig. S6†) do not contain any signal for aluminium or for any other cation suggests that the surface is dominated by hydrogen phosphates, with the consistent O : P ratio of 3 : 1 indicating extensive polymerization at the surface. We also note that no XPS signal due to chlorine is observed for any of the samples (Fig. S7†). Following annealing at 800 °C, the samples from all precursors are highly crystalline, and the presence of the Al(2p) peak in the XP spectra suggests that the surface is now dominated by aluminium metaphosphate. However, the P : Al ratio remains higher than the expected 3 : 1 ratio, particularly for  $\text{AlCl}_3(800)$ , suggesting that some hydrogen polyphosphates are present at the surface.

#### Surface analysis with ATR-FTIR

The sampling depth of ATR-FTIR spectroscopy, typically between 0.5–2  $\mu\text{m}$ , is significantly larger than that for XPS, which detects only the top 2–4 nm of the surface for the elements studied here. Nevertheless, there is excellent agreement between the IR results and the results from the more surface sensitive XPS method, as illustrated in Fig. 7, which shows FTIR data for several samples.



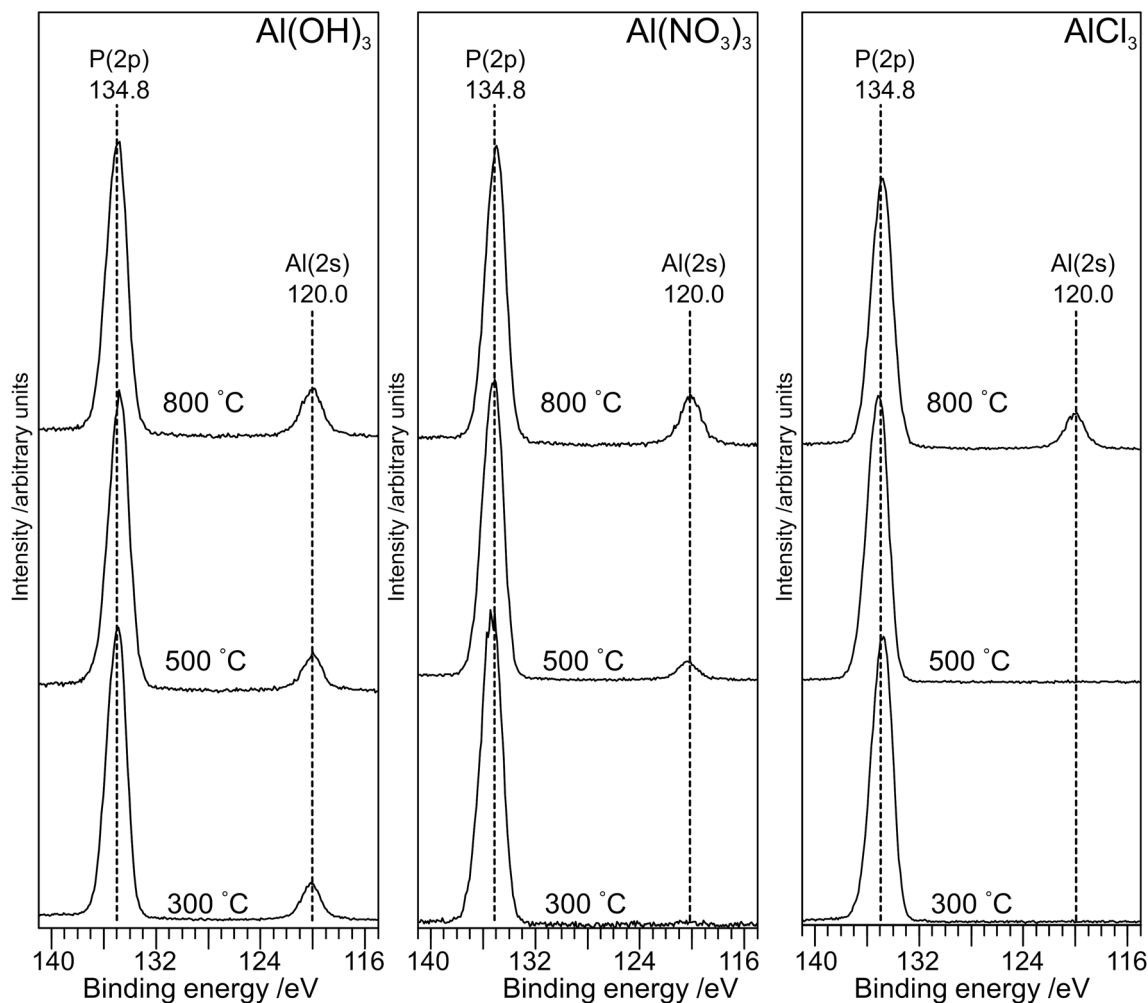


Fig. 6 X-ray photoelectron spectra in the P(2p) and Al(2s) region for the aluminium phosphate materials prepared from the  $\text{Al}(\text{OH})_3$ ,  $\text{Al}(\text{NO}_3)_3$  and  $\text{AlCl}_3$  precursors at different annealing temperatures. For all three precursors, a small shift ( $\sim 0.2$  eV) to lower binding is observed on annealing at  $800^\circ\text{C}$ .

For  $\text{AlPO}_4(300)$ , broad, weak bands are present in the range *ca.*  $1100\text{--}1250\text{ cm}^{-1}$ , characteristic of an aluminium orthophosphate with some indication of P–O–P bond formation from the weak peak at  $1025\text{ cm}^{-1}$ .<sup>18</sup> The spectra for  $\text{AlPO}_4(500)$  and  $\text{AlPO}_4(800)$  are dominated by strong bands assigned to metaphosphates. In particular, the peak at  $738\text{ cm}^{-1}$  is assigned to Al–O–P, bands at  $811$ ,  $1025$ ,  $1060$  and  $1070\text{ cm}^{-1}$  are assigned to P–O–P modes, and bands at  $1282$  and  $1305\text{ cm}^{-1}$  are assigned to P=O bonds in the aluminium metaphosphate.

## Discussion

The structures of aluminium orthophosphate, aluminium hexacyclopentaphosphate and two aluminium metaphosphates are shown in Fig. 3, and can be used to rationalize the changes in the XP spectra observed for different annealing temperatures. Small shifts to lower binding energy are observed for the P(2p) and Al(2p) peaks as the annealing temperature is increased, but the most significant changes arise in the O(1s) spectra, which show a transfer of intensity from a higher binding energy peak at

$533.7\text{ eV}$  to a lower binding energy peak at  $532.3\text{ eV}$ . The best starting point to understand these changes is the O(1s) spectra for all samples annealed at  $800^\circ\text{C}$ , as these spectra are all very similar to those reported by several other authors, including Gresch *et al.* for sodium metaphosphates,<sup>8</sup> Crobu *et al.* for zinc phosphates,<sup>9</sup> and Rotole and Sherwood for model aluminium phosphates.<sup>11,12</sup> The FTIR, XRD and solid-state  $^{31}\text{P}$  NMR data indicate the presence of mainly cubic aluminium metaphosphate after annealing at  $800^\circ\text{C}$  and we can therefore definitively assign the peaks in the O(1s) region at  $533.7\text{ eV}$  and  $532.3\text{ eV}$ , respectively, to oxygen atoms bridging between phosphorus atoms (P–O–P) and oxygen atoms bridging between phosphorus and aluminium atoms (P–O–Al), in agreement with Gresch *et al.*

In the metaphosphate, these two bonding environments are expected to be present in a 2 : 1 ratio of P–O–Al to P–O–P. However, as shown in Table 1, quantification of the XPS data for the samples annealed at  $800^\circ\text{C}$  gives a peak area ratio ( $532.3\text{ eV} : 533.7\text{ eV}$ ) of *ca.* 1.6 : 1, whereas the expected ratio is 2 : 1. Thus, the P : Al ratio at the surface of these materials is higher than the expected 3 : 1 ratio. To understand these differences,



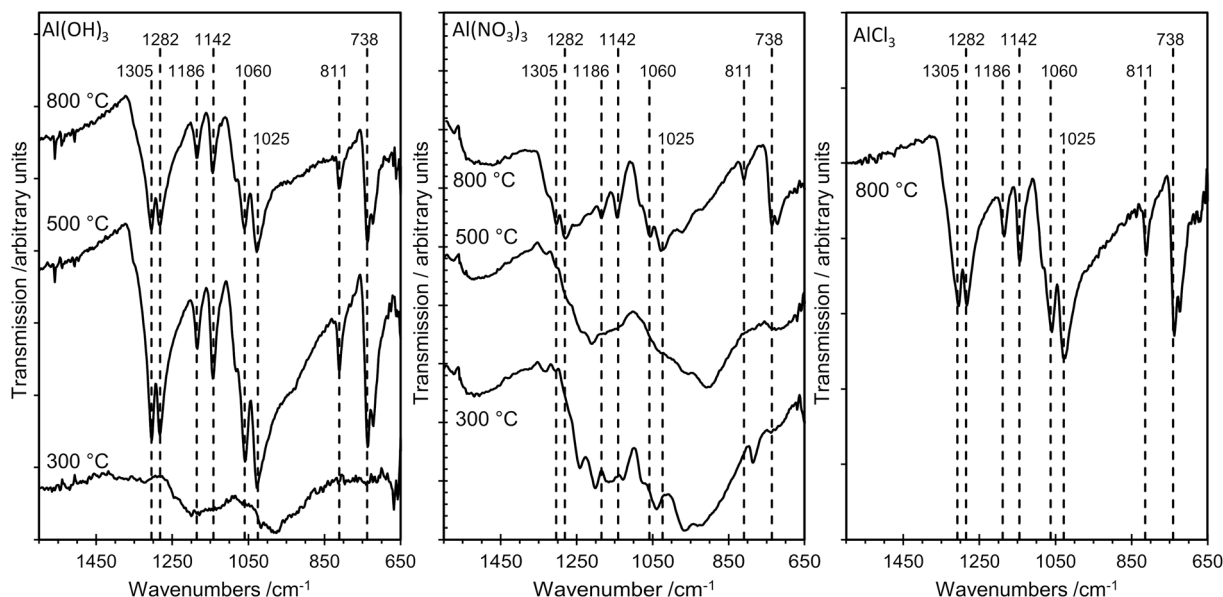


Fig. 7 ATR-FTIR spectra of the aluminium phosphate materials prepared from the  $\text{Al}(\text{OH})_3$ ,  $\text{Al}(\text{NO}_3)_3$  and  $\text{AlCl}_3$  precursors at different annealing temperatures. At 300 °C the poorly resolved spectra are characteristic of aluminium orthophosphate, whereas aluminium metaphosphate dominates at 500 °C and 800 °C. The materials prepared from the  $\text{AlCl}_3$  precursor did not crystallize at the lower annealing temperatures, and ATR spectra were only recorded for the sample annealed at 800 °C.

we now consider the XP spectra recorded for samples annealed to lower temperatures.

A key observation is that the  $\text{AlP}_{\text{NO}_3}(300)$  and  $\text{AlP}_{\text{Cl}}(300)$  samples show no evidence, in the XP spectra, for the presence of aluminium. The  $\text{AlP}_{\text{NO}_3}(500)$  sample does show evidence for aluminium, but the  $\text{AlP}_{\text{Cl}}(500)$  sample does not. The absence of aluminium indicates a purely hydrogen terminated phosphate material at the surface. Unreacted phosphoric acid can be ruled out based on the O : P ratio of 3 : 1, but there is evidence from the solid-state  $^{31}\text{P}$  NMR results for hydrogen terminated or cyclic polyphosphates (giving peaks at  $-28$  ppm and  $-32$  ppm) which would have a 3 : 1 ratio. A cyclic polyphosphate such as  $\text{P}_4\text{O}_{10}$  has a P–O–P to P=O bond ratio of 1.5 : 1, which could account for the XPS ratios if the oxygen in P=O has a binding energy of  $\sim 532$  eV, overlapping with the XPS peak for the oxygen in P–O–Al. This assignment would be in agreement with Gresch *et al.*<sup>8</sup> Finally, the “wet” physical appearance of samples annealed at lower temperatures is also consistent with the presence of hydrogen polyphosphates which would be poorly crystalline.

From the data presently available, we cannot determine whether annealing ultimately leads to sublimation or decomposition of the polymeric phosphates, or whether further reaction with unreacted aluminium precursor occurs. However, for samples annealed at 800 °C, the XP spectra are consistent with the presence of aluminium metaphosphates although the slightly higher P : Al ratio in the case of the material prepared from  $\text{AlCl}_3$  suggests the surface contains some hydrogen terminated polyphosphates.

## Conclusions

Aluminium metaphosphate is formed from the reaction of phosphoric acid with three different aluminium compounds

( $\text{Al}(\text{OH})_3$ ,  $\text{Al}(\text{NO}_3)_3$  and  $\text{AlCl}_3$ ) followed by annealing in air. XRD, XPS and FTIR measurements of the resulting materials show almost identical behaviour from all three precursors, but the solid-state  $^{31}\text{P}$  NMR spectra are significantly different at the lower annealing temperatures (300 °C and 500 °C). The unique solid-state  $^{31}\text{P}$  NMR spectra of the materials annealed at lower temperatures indicates the presence of amorphous materials which would not be identified by XRD, but explains the lack of an Al(2p) signal in XP spectra of the materials prepared from the  $\text{Al}(\text{NO}_3)_3$  and  $\text{AlCl}_3$  precursors at lower annealing temperatures. For all three precursors, a cubic metaphosphate is produced on annealing at 800 °C, with a hexacyclophosphate present at lower annealing temperatures in the case of the  $\text{Al}(\text{NO}_3)_3$  and  $\text{Al}(\text{OH})_3$  precursors. The XP spectra in the O(1s) region of the aluminium phosphate materials show two components at 532.3 eV and 533.7 eV, which are definitively assigned to the P–O–Al and P–O–P bonding environments, respectively. However, samples annealed at lower temperatures also exhibit surface species assigned as cyclic polyphosphates, with binding energies of 532.3 eV and 533.7 eV for the P=O and P–O–P bonding environments, respectively.

## Conflicts of interest

There are no conflicts to declare.

## Acknowledgements

VB, MT and LE are grateful for studentships funded by Cogent Power Ltd. XP spectra were recorded by the EPSRC National Facility for Photoelectron Spectroscopy (HarwellXPS), operated by Cardiff University and UCL under contract number PR16195. The UK 850 MHz solid-state NMR Facility used in this research





was funded by EPSRC and BBSRC (contract reference PR140003), as well as the University of Warwick including via part funding through Birmingham Science City Advanced Materials Projects 1 and 2 supported by Advantage West Midlands (AWM) and the European Regional Development Fund (ERDF).

## Notes and references

- 1 S. V. Dorozhkin and M. Epple, *Angew. Chem., Int. Ed.*, 2002, **41**, 3130–3146.
- 2 M. Nabiyouni, T. Brueckner, H. Zhou, U. Gbureck and S. B. Bhaduri, *Acta Biomater.*, 2018, **66**, 23–43.
- 3 M. Nabiyouni, Y. Ren and S. B. Bhaduri, *Mater. Sci. Eng., C*, 2015, **52**, 11–17.
- 4 X. Yu, C. Qian and X. Wang, *Sci. Adv. Mater.*, 2015, **7**, 1730–1733.
- 5 Y. N. Trepalina, V. A. Doroganov and E. I. Evtushenko, *Refract. Ind. Ceram.*, 2011, **52**, 291–293.
- 6 F. Rashchi and J. A. Finch, *Miner. Eng.*, 2000, **13**, 1019–1035.
- 7 R. N. Panda, M. F. Hsieh, R. J. Chung and T. S. Chin, *J. Phys. Chem. Solids*, 2003, **64**, 193–199.
- 8 R. Gresch, W. Muller-Warmuth and H. Dutz, *J. Non-Cryst. Solids*, 1979, **34**, 127–136.
- 9 M. Crobu, A. Rossi, F. Mangolini and N. D. Spencer, *Anal. Bioanal. Chem.*, 2012, **403**, 1415–1432.
- 10 J. A. Rotole and P. M. A. Sherwood, *Chem. Mater.*, 2001, **13**, 3933–3942.
- 11 J. A. Rotole and P. M. A. Sherwood, *Surf. Sci. Spectra*, 1998, **5**, 60–66.
- 12 J. A. Rotole and P. M. A. Sherwood, *Surf. Sci. Spectra*, 1998, **5**, 67–74.
- 13 N. Fairley, *CasaXPS Manual: 2.3.15 Spectroscopy*, Casa Software Ltd, 2009.
- 14 F. d'Yvoire, *Bull. Soc. Chim. Fr.*, 1961, 1762.
- 15 F. d'Yvoire, *Bull. Soc. Chim. Fr.*, 1961, 2277.
- 16 G. Tricot, D. Coillot, E. Creton and L. Montagne, *J. Eur. Ceram. Soc.*, 2008, **28**, 1135–1141.
- 17 NIST X-ray Photoelectron Spectroscopy Database, Version 4.1, National Institute of Standards and Technology, Gaithersburg, 2012, <http://srdata.nist.gov/xps/>.
- 18 D. Wang, Y. Xu, L. Yang, F. Wang, A. M. Asiri and K. A. Alamry, *J. Mol. Liq.*, 2018, **258**, 327–334.

